

# Memoryless Quantum Repeaters Based on Cavity-QED and Coherent States

Pei-Zhe Li\* and Peter van Loock\*

A quantum repeater scheme based on cavity-quantum electrodynamics (QED) and quantum error correction of channel loss via rotation-symmetric bosonic codes (RSBCs) is proposed to distribute atomic entangled states over long distances without memories and at high clock rates. In this scheme, controlled rotation gates, i.e., phase shifts of the propagating light modes conditioned upon the state of an atom placed in a cavity, provide a mechanism both for the entangled-state preparations and for the error syndrome identifications. In order to assess the performance of this repeater protocol, an explicit instance of RSBCs—multicomponent cat codes—are studied quantitatively. It is found that the total fidelity and the success probability for quantum communication over a long distance (such as 1000 km) both can almost approach unity provided a small enough elementary distance between stations (smaller than 0.1 or 0.01 km) and rather low local losses (up to 0.1%) are considered. In a quantum key distribution application, secret key rates can become correspondingly high, both per channel use, beating the repeaterless bound, and per second thanks to the relatively high clock rates of the memoryless scheme. Based upon the cavity-QED setting, this scheme can be realized at room temperature and at optical frequencies.

## 1. Introduction

One of the key topics in quantum information processing recently is quantum communication over long distances, beyond what is achievable in a so-called point-to-point link via direct optical state transmission. In order to obtain high fidelities and rates (or secret key rates in quantum key distribution (QKD)), the exponential decrease of these quantities with distance, caused by the lossy bosonic channel (LBC) representing an optical fiber, must be suppressed. The most common and best known approach to remedy this fundamental scaling problem of fiber-based quantum communication is the so-called quantum repeater in which an otherwise long-distance point-to-point communication channel is divided into shorter segments.<sup>[1,2]</sup> The intermediate repeater stations are then equipped with stationary matter qubits that can couple to the incoming, flying photonic qubits, temporarily store and release them. Based on this, the typically heralded distribution

of entangled photon pairs can be synchronized among all the repeater segments and these short-distance pairs can then be connected via quantum teleportation (entanglement swapping). In order for this scheme to be really scalable to larger distances, additional steps of entanglement distillation are needed to suppress the accumulation of memory and gate errors.


This standard quantum repeater based on quantum memories and probabilistic entanglement distillation, though scalable in principle, has a couple of complications. While the requirement of an efficient, long-lasting quantum memory system is of more technical, experimental nature, a more conceptual and fundamental issue is the need for two-way classical communication in such repeaters, even over distances beyond those of the elementary segment lengths, significantly limiting the possible final rates. The use of quantum error correction codes for the matter qubits allows to circumvent the need for probabilistic operations on higher nesting levels of a quantum repeater link and hence for any two-way classical communication between non-nearest repeater stations.<sup>[3]</sup> While this approach helps to enhance the final rates in principle, it still requires quantum memories and two-way classical communication for the initial encoded, entangled state distributions and distillations. Instead, a more recent concept would rather avoid the need for quantum memories and two-way classical communication entirely by minimizing the effect of the LBC through certain optical encodings, i.e., photonic

P.-Z. Li, P. van Loock  
Institut für Physik  
Johannes Gutenberg-Universität Mainz  
Staudingerweg 7, 55128 Mainz, Germany  
E-mail: peili@nii.ac.jp; loock@uni-mainz.de

P.-Z. Li  
Department of Informatics  
School of Multidisciplinary Sciences, SOKENDAI (The Graduate University for Advanced Studies)  
2-1-2 Hitotsubashi, Chiyoda-ku, Tokyo 101-8430, Japan

P.-Z. Li  
National Institute of Informatics  
2-1-2 Hitotsubashi, Chiyoda-ku, Tokyo 101-8430, Japan

P.-Z. Li  
Quantum Information Science and Technology Unit  
Okinawa Institute of Science and Technology (OIST) Graduate University  
Okinawa 904-0495, Japan

 The ORCID identification number(s) for the author(s) of this article can be found under <https://doi.org/10.1002/qute.202200151>

© 2023 The Authors. Advanced Quantum Technologies published by Wiley-VCH GmbH. This is an open access article under the terms of the Creative Commons Attribution License, which permits use, distribution and reproduction in any medium, provided the original work is properly cited.

DOI: 10.1002/qute.202200151

or, more generally, bosonic quantum error correction codes that protect a bosonic mode from loss.<sup>[4]</sup> In this case, the clock rate of the repeater scheme is no longer determined by any classical-signal waiting times, but solely depends on the longest time duration required for the local processing at any repeater station. The motivation of this work is to propose and assess a similar, memoryless repeater scheme for long-distance quantum communication making use of “Schrödinger cat states” for bosonic quantum error correction (QEC) in order to improve the fidelities and the rates.

The cat code<sup>[5]</sup> is a prime example of a bosonic code where a logical qubit is encoded in an oscillator mode. Thus, it is sometimes also referred to as an instance of a continuous-variable (CV) code. It has been proposed in particular to correct photon loss occurring on the bosonic mode exploiting certain photon number parity properties of suitable cat states. With the help of cavity-quantum error distribution (QED), cat states can be deterministically generated at room temperature in the laboratory.<sup>[6]</sup> Our work is especially based on the idea that the experimental scheme<sup>[6]</sup> could not only be used to generate (atom–light entangled) cat states, but also to do the syndrome detections for cat code error correction. Using this method, it is possible to construct a model of quantum repeaters that do not require any memories or two-way classical communications. More generally, it is possible to extend the simplest instance of such a scheme to create multicomponent cat states, which can be used for quantum error correction with higher-loss cat codes.<sup>[7,8]</sup> There also exists a more general class of quantum states and codes compared to that of multicomponent cat states or codes. These more general codes are referred to as “rotation-symmetric bosonic codes” (RSBCs) and they exhibit, like the “cat states”, rotational symmetries in phase space.<sup>[9]</sup> We will argue that, in principle, all the above-mentioned operations for “cat states” also work for the generalized class of states. First, we can physically prepare these states in the lab given that we are able to create a corresponding “primitive state”, which is useful in the context of quantum computing.<sup>[9]</sup> Second, these states are also potentially useful in long-distance quantum communication in the same way as the cat codes. Nonetheless, here our quantitative analysis will focus on cat codes and we shall not explicitly assess the performance of the generalized states, even though they could help to enhance the performance beyond that of cat codes. For the cat codes, however, we will systematically derive and quantitatively assess instances of the higher-order loss codes<sup>[7,8]</sup> spanned by more than those four distinct coherent states as for the original one-loss cat code.<sup>[5]</sup> While there are all-optical proposals for state generation and error correction with four coherent states,<sup>[10–12]</sup> it is unclear whether and how these are extendible to the regime of higher-loss codes with more coherent states.

Compared with most existing schemes for fast, memoryless quantum communication or so-called 3rd-generation quantum repeaters<sup>[4]</sup> where logical qubits are encoded in many physical, photonic qubits, and twice as many optical modes, our scheme is particularly “hardware-efficient” from the perspective of optics by exploiting bosonic single-mode codes that are sent through the fiber channel. To some extent, this concept has already been explored,<sup>[7,8]</sup> but an explicit optical realization has not been considered yet. Other existing approaches for fast, long-distance quantum communication rely upon a different, shift-invariant

class of bosonic codes that also encode logical qubits into oscillator modes,<sup>[13]</sup> but partially also make use of concatenations with higher-level qubit codes.<sup>[14,15]</sup> An experimental complication in these schemes, however, is that it is even hard to create the corresponding low-level code states in the optical regime, although also for this proposals based on cavity-QED exist.<sup>[16]</sup> For logical qubits encoded into cat states, it may also be useful to protect the cat qubits through higher-level qubit quantum error correction codes.<sup>[12,17,18]</sup> While this can lead to a further improvement of the possible (secret key) rates, it would also render the state generations and encoding circuits more complicated and, by relying upon many optical modes for the total code states, it would go beyond the efficient bosonic single-mode encoding and transmission.

Our cat code repeater scheme, though functioning without qubit storage and two-way classical communication, does require atomic qubits at each repeater station for the local state preparations and the error correction operations. Therefore, it cannot simply be operated at the potentially very fast clock rate of a laser source or an optical quantum state preparation device. Instead, the elementary time units of our scheme are determined by the speed of the local atom–light operations (typically operating at MHz rates). Another limiting factor will be the small repeater spacing, which is required for the bosonic quantum error correction that works best at sufficiently small channel loss. In this case, the local experimental imperfections of the atom–light system at each repeater station will accumulate more heavily. Here we model these local imperfections of the cavity-QED system at each station as an additional constant loss which primarily includes atomic loss (spontaneous decay) and coupling inefficiencies between the cavity-QED and fiber communication systems. There is no time dependence of the local loss, since it is not associated with a variable memory decay in our memoryless scheme. Nonetheless, local loss is a bottle neck in our scheme, because it must be very small in order to allow for the frequent error correction steps along the channel in our cavity-QED-based repeater scheme.

## 2. Background and Methods

In this section, we present some background material and methods as needed for our quantum communication scheme. This includes some notions and specific interactions of cavity-QED, cavity-QED-based procedures to create entangled atom–light and eventually atom–atom states and also to do syndrome measurements for quantum error correction. We shall also discuss the effect of loss channels on these entangled states.

### 2.1. Methods from Cavity-QED

It has been shown both in theory<sup>[19,20]</sup> and in experiment<sup>[6]</sup> that so-called even or odd cat states (quantum superposition of optical coherent states) can be generated with the help of a high-finesse cavity containing a single trapped atom. The trapped atom consists of three relevant levels. Two of them are the ground state,  $|\uparrow\rangle$  and  $|\downarrow\rangle$ , the remaining one is the excited state,  $|e\rangle$ . The transition  $|\uparrow\rangle \rightarrow |e\rangle$  is strongly coupled to the bare cavity mode. The

transition  $|\downarrow\rangle \rightarrow |e\rangle$  is decoupled from the cavity mode because of the energy gap between the two (hyperfine and, possibly, Zeeman) ground states. Then one may consider the scenario that an input light field, which is resonant with the cavity mode is reflected from the cavity. If the atom is prepared in state  $|\uparrow\rangle$ , then due to the strong coupling of the cavity and the atom, the frequency of the dressed cavity mode will be significantly detuned from that of the input light. In this case the reflection becomes similar to the reflection from a mirror, which keeps the input state of light unchanged. If the atom is prepared in state  $|\downarrow\rangle$ , the input light mode is strongly coupled with the cavity mode, so after the reflection, the output mode will acquire an extra phase of  $e^{i\pi}$ . However, if the light mode is not perfectly resonant with the cavity mode, i.e., there is a photon energy/frequency detuning  $\Delta$  between them, the extra phase becomes different from  $e^{i\pi}$ . According to the quantum optics calculation, the relation between the input and the output light mode operators is<sup>[19]</sup>

$$\hat{a}_{\text{out}} \approx \frac{i\pi\Delta - \frac{\kappa}{2}}{i\pi\Delta + \frac{\kappa}{2}} \hat{a}_{\text{in}}, \quad (1)$$

where  $\kappa$  is the cavity decay rate. This relation corresponds to the rotation operator

$$\hat{R}(\phi) = \exp(i\phi\hat{n}) \quad (2)$$

acting on the state of the input light mode, where  $\hat{n} = \hat{a}^\dagger \hat{a}$  is the photon number operator and the rotation angle  $\phi = \arg((i\pi\Delta - \frac{\kappa}{2})/(i\pi\Delta + \frac{\kappa}{2}))$ . With this quantum gate for optical modes, we are able to create states with rotational symmetries. Moreover, as explained in detail below, for quantum error correction using certain suitably encoded states, this operation can extract information that tells us which error space a state belongs to. This kind of information is part of the syndrome measurement, which is crucial to enhance fidelities when the states are subject to errors. Finally, this provides a possibility to generate entanglement probabilistically after an appropriate measurement, for instance, via unambiguous state discrimination (USD) or homodyne detection.

In experiments, there are more parameters related to the rotation angle  $\phi$  and the amplitude will be damped slightly after the reflection because of the inevitable losses.<sup>[6]</sup> The respective complex reflection amplitude  $r$  including additional parameters is<sup>[6]</sup>

$$r(\Delta) = 1 - \frac{2\kappa_r(2i\pi\Delta + \gamma)}{(2i\pi\Delta + \kappa)(2i\pi\Delta + \gamma) + g^2}. \quad (3)$$

where  $\kappa_r/\kappa$  is the reduced escape efficiency of the cavity, which does not reflect all of the incoming light (due to optical scattering into modes distinct from the reflected target mode). The parameter  $\gamma$  is the atomic dipole decay rate and  $g$  is the atom-cavity coupling constant. Then the relative phase shift is given by  $\phi(\Delta) = \arg(r(\Delta)|_{g=0}) - \arg(r(\Delta)|_{g=g_0})$ ,<sup>[6]</sup> where  $g_0 = 2\pi \times 7.8$  MHz is the value of  $g$  for the coupling case.<sup>[6]</sup> We set these parameters to be the same as given by Hacker et al.<sup>[6]</sup> in **Figure 1** for what we call the “practical” curves.

Based on this, let us briefly discuss the different regimes for the conditional phase rotation depending on the experimental pa-

rameters including, especially, the chosen regime for the detuning. Importantly, we shall argue that for our repeater scheme to be operated using these interactions from cavity-QED, all cavities can be employed in a regime where the rotation angle  $\phi$  is between  $\pi/2$  and  $\pi$ . In this case, the simple theoretical model matches recent experiments<sup>[6]</sup> and amplitude damping can be avoided to a great extent.

From Figure 1a, one can see that with proper parameters (to be more specific, it is required that  $g^2 \gg \kappa\gamma$ ,  $\kappa_r \approx \kappa$ , and  $-3$  MHz  $< \Delta < 3$  MHz), a phase shift between  $\pi/2$  and  $3\pi/2$  can be reached and the “practical” and idealized theoretical (without amplitude damping) curves basically coincide. Later, in order to describe our repeater protocol, initially we will assume perfect local operations (no local loss) and subsequently, in the rate analysis part, we will also consider the local losses including the amplitude damping as represented by Equation (3). Figure 1 further illustrates and implies (see Figure 1b,c) that, both for the theoretical approximation and in practice (“practical”), in order to get a small phase shift approaching zero, one needs a rather large detuning, beyond 7 MHz. In this regime, the theoretical and “practical” curves no longer coincide, although both give decreasing phase shifts approaching zero with large detuning. This general behavior can also be inferred from the theoretical expression for the rotation angle  $\phi = \arg((i\pi\Delta - \frac{\kappa}{2})/(i\pi\Delta + \frac{\kappa}{2}))$ . Related with these discrepancies, at around  $\Delta = 7.5$  MHz the “practical” scheme can lead to a significantly reduced amplitude of the scattered light field (see Figure 1c). Even though the phase shift can be small and close to zero when  $\Delta \approx 7.5$  MHz in “practical”, the modulus of the amplitude for the coupling case ( $g = g_0$ ) becomes too small with this value of  $\Delta$ . When the detuning reaches 15 MHz or beyond, small phase shifts in combination with an invariant amplitude (no amplitude reduction) can always be obtained (in both practice and theory). However, we stress that such a large detuning is unnecessary for our repeater scheme to work. While we should certainly avoid the  $\Delta$ -regime in the range  $3$  MHz  $< \Delta < 10$  MHz, based on the above discussion, we could choose between the regimes  $-3$  MHz  $< \Delta < 3$  MHz and, e.g.,  $\Delta > 10$  MHz. Avoiding the use of too large detuning, it may then be more feasible experimentally to have  $\Delta$  in the range of 0 MHz  $< \Delta < 3$  MHz with phase shifts near  $\pi/2$  and bigger, up to  $\pi$ . In the following, however, for simplicity, we make use of cavities with a rotation angle  $\phi$  smaller than  $\pi/2$ . Thanks to the rotational symmetry of the RSBCs considered in this paper, the use of a cavity with rotation angle  $\phi$  is equivalent to the use of a cavity with rotation angle  $\pi - \phi$  in our repeater scheme (details are given in Section S2, Supporting Information). Therefore, all cavities can be replaced by those with  $\phi$  bigger than  $\pi/2$  and smaller than  $\pi$ , which is precisely the regime that works very well according to the above discussion. Thus, all the arguments in this section are still valid, provided the discussions here and as presented in Section S2 of the Supporting Information are taken into account with regards to real experiments.

In the next three subsections, we first consider only a single repeater segment to do the quantum error correction and finally create the entanglement. Quantum memories may be present at the station that sends the light mode (Alice). If we want to create entanglement shared between Alice and Bob and keep it for certain applications, we need another quantum memory at the station receiving the light mode (Bob). However, in our final,

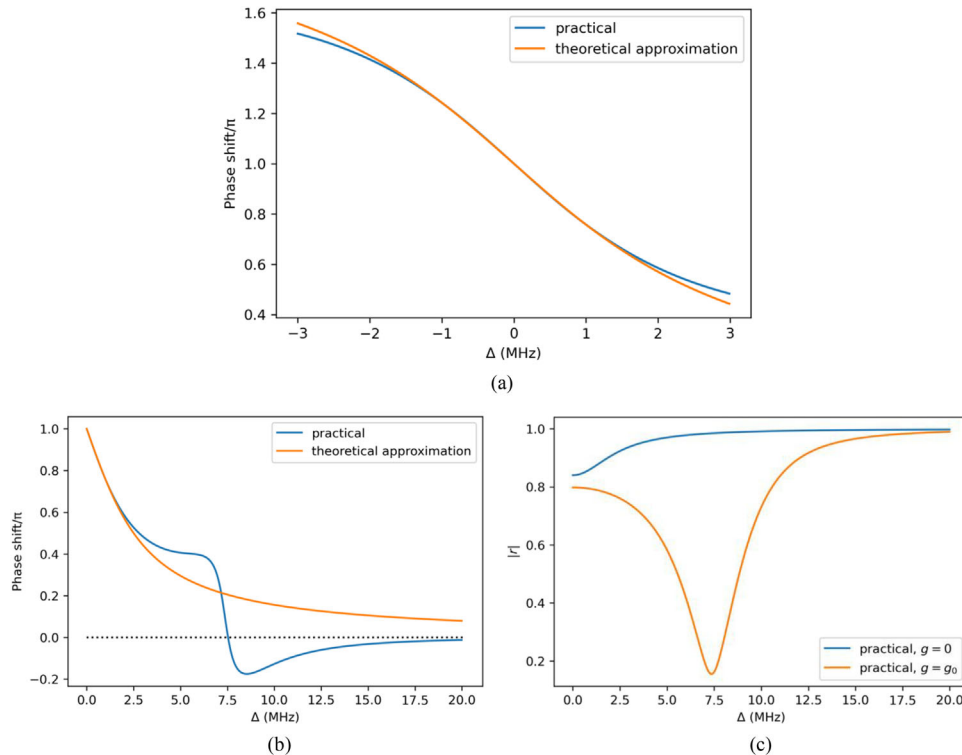


**Figure 1.** a,b) The phase shift caused by the light–matter interaction as a function of the photon energy/frequency detuning  $\Delta$ . The orange curve is the theoretical approximation which keeps the modulus of the amplitude unchanged. The blue curve is more accurate, including more experimental (“practical”) parameters, but in this case the amplitude can be reduced. c) The corresponding modulus of the reflection amplitudes with  $g = 0$  and  $g = g_0 = 2\pi \times 7.8$  MHz.

complete quantum repeater scheme, connecting many such elementary segments, the overall procedure can be done without quantum memories and only the entangled pairs in Alice and Bob’s hands may be kept. When the specific application is QKD, Alice’s atom can be measured once the desired code states are available at the station sending the light mode. Similarly, also Bob’s atom can be measured immediately after all the necessary light–atom interactions at the station receiving the light mode. So, no quantum memories are needed at all (even for Alice and Bob) for QKD. Our theoretical analysis and all derivations are independent of the particular choice of application (see Section 3.1 and Section S7 (Supporting Information) for details). Hence it works for both long-range QKD and applications that rely on long-distance stationary entanglement distribution between Alice and Bob.

## 2.2. State Preparation

The cavity-QED-based, detuning-dependent phase rotation method as described in Section 2.1 provides a realization for a kind of “hybrid controlled rotation gate”. Here “hybrid” means that the controlling part is the atomic state and the target part is the light mode, and so the gate performs a hybrid operation between the atomic state and the incident light mode. Similarly, the gate is expressible by discrete-variable qubit operators acting on the atom and CV oscillator (“qumode”) operators acting

on the light field mode. With the help of this gate, we can easily generate states with discrete rotation symmetry. First, we prepare the atom as mentioned above in a superposition of the two ground states,  $(|\uparrow\rangle + |\downarrow\rangle)/\sqrt{2}$ , and then reflect an arbitrary light-mode state  $|\Theta\rangle$  from the cavity. Then, as mentioned before, the light-mode state  $|\Theta\rangle$  will be either rotated in phase space or remain the same depending on the state of the atom either in  $|\uparrow\rangle$  or  $|\downarrow\rangle$

$$\begin{aligned} |\uparrow\rangle|\Theta\rangle &\rightarrow |\uparrow\rangle|\Theta\rangle, \\ |\downarrow\rangle|\Theta\rangle &\rightarrow |\downarrow\rangle\hat{R}(\phi)|\Theta\rangle. \end{aligned} \quad (4)$$

This action can be formally expressed as a hybrid controlled rotation (hCROT) gate acting jointly on an atomic and a light-mode input state

$$hCROT_\phi = |\uparrow\rangle\langle\uparrow| \otimes \hat{1} + |\downarrow\rangle\langle\downarrow| \otimes \exp(i\phi\hat{n}). \quad (5)$$

To create a state of light with  $2^m$ -fold rotation symmetry ( $2^m$ -fold as adapted to our specific encoded state preparation method), at first we need to set the rotation angle  $\phi = \pi$ , which can be realized by setting the detuning  $\Delta = 0$ . Thus, after the first reflection, the state becomes

$$\frac{1}{\sqrt{2}} \left( |\uparrow\rangle|\Theta\rangle + |\downarrow\rangle\hat{R}(\pi)|\Theta\rangle \right), \quad (6)$$

so the atom and the light mode become entangled. We can then rewrite the state

$$\begin{aligned} & \frac{1}{\sqrt{2}} \left( |\uparrow\rangle |\Theta\rangle + |\downarrow\rangle \hat{R}(\pi) |\Theta\rangle \right) \\ &= \frac{1}{2} \left[ \frac{1}{\sqrt{2}} (|\uparrow\rangle + |\downarrow\rangle) \left( |\Theta\rangle + \hat{R}(\pi) |\Theta\rangle \right) \right. \\ & \quad \left. + \frac{1}{\sqrt{2}} (|\uparrow\rangle - |\downarrow\rangle) \left( |\Theta\rangle - \hat{R}(\pi) |\Theta\rangle \right) \right]. \end{aligned} \quad (7)$$

Next, after doing a projective measurement of the atomic state in the basis  $\{|\pm\rangle\} = (|\uparrow\rangle \pm |\downarrow\rangle) / \sqrt{2}$ , the state of light will be projected onto a superposition of  $|\Theta\rangle$  and the rotated state  $\hat{R}(\pi)|\Theta\rangle$ , i.e.,  $|\Theta\rangle \pm \hat{R}(\pi)|\Theta\rangle$  (unnormalized). This step has already been realized in the lab with  $|\Theta\rangle = |\alpha\rangle$ , generating the even or odd “cat states”  $(|\alpha\rangle \pm |-\alpha\rangle) / N_{\pm}$ , where  $N_{\pm}$  is the normalization constant.<sup>[6]</sup> As a next step, we adjust the cavity (or prepare another cavity) to make the detuning  $\Delta = \kappa/2$ , so the rotation angle  $\phi$  becomes  $\pi/2$ , and we prepare the atom inside again in the state  $(|\uparrow\rangle + |\downarrow\rangle) / \sqrt{2}$ . Assuming we obtain  $|\Theta\rangle + \hat{R}(\pi)|\Theta\rangle$  from the first step, then if we reflect this state again from the adjusted cavity (or another cavity), we will get the light state

$$|\Theta\rangle + \hat{R}(\pi) |\Theta\rangle \pm \hat{R}\left(\frac{\pi}{2}\right) |\Theta\rangle \pm \hat{R}\left(\frac{3\pi}{2}\right) |\Theta\rangle \quad (8)$$

after the projective measurement of the atomic state similar to the first step.<sup>[21]</sup> Repeating the steps above and adjusting the cavity (or preparing another cavity) in every step with the rotation angle  $\phi$  being half of the angle from the previous step, finally, the joint atom–light state (before the atomic measurement) will become

$$\frac{1}{\sqrt{2}} \left( |\uparrow\rangle |0_{2^m, \Theta}\rangle + |\downarrow\rangle |1_{2^m, \Theta}\rangle \right), \quad (9)$$

$\forall m \in N_0$  after  $m + 1$  steps, where

$$\begin{aligned} |0_{M, \Theta}\rangle &= \frac{1}{\sqrt{N_M}} \sum_{k=0}^{M-1} \hat{R}\left(\frac{2k\pi}{M}\right) |\Theta\rangle, \\ |1_{M, \Theta}\rangle &= \frac{1}{\sqrt{N_M}} \sum_{k=0}^{M-1} \hat{R}\left(\frac{(2k+1)\pi}{M}\right) |\Theta\rangle, \end{aligned} \quad (10)$$

with a normalization constant  $N_M$ . The two states  $|0_{M, \Theta}\rangle$  and  $|1_{M, \Theta}\rangle$  are the logical codewords used in our scheme. Both of them exhibit rotation symmetry, i.e.,

$$\begin{aligned} \hat{R}\left(\frac{2\pi}{M}\right) |0_{M, \Theta}\rangle &= |0_{M, \Theta}\rangle, \\ \hat{R}\left(\frac{2\pi}{M}\right) |1_{M, \Theta}\rangle &= |1_{M, \Theta}\rangle. \end{aligned} \quad (11)$$

Equation (10) is the general definition of the two codewords of a rotation-symmetric bosonic qubit code for any integer  $M$ . However, according to Equation (9), the above method can only generate states for  $M = 2^m$ .

Here the codewords are generally not orthogonal,  $\langle 0_{M, \Theta} | 1_{M, \Theta} \rangle \neq 0$ . Nevertheless, the logical codewords can also be con-

structed to be orthogonal.<sup>[9]</sup> For example, the two orthogonal states  $|\Theta\rangle + \hat{R}(\pi)|\Theta\rangle$  and  $|\Theta\rangle - \hat{R}(\pi)|\Theta\rangle$  (unnormalized) in Equation (7) can also be used as the codewords. Although the orthogonal codewords can be discriminated deterministically (at least in theory), they cannot lead to a deterministic entanglement creation process, because one has to add two different normalization constants to normalize the two states and the difference will finally make the process probabilistic again. A more detailed discussion can be found in Section S3 of the Supporting Information.

### 2.3. Syndrome Measurement

QEC is essential to suppress the errors, in our case, primarily related with the LBC. In order to correct the errors, a syndrome measurement is necessary, which extracts the error information from the encoded state.

After preparing the state in Equation (9) in the desired loss order (the loss order  $L = 2^m - 1$  for  $|0_{M, \Theta}\rangle$  and  $|1_{M, \Theta}\rangle$ ), “Alice” transmits the light mode via an optical fiber.<sup>[22]</sup> Inevitably, some photons will get lost during the transmission. Before considering the full loss channel, it is conceptually useful to first think of a simplified loss channel, where we only apply the annihilation operator  $\hat{a}$  to the codewords. The number of losses then corresponds to the powers of  $\hat{a}$ . The resulting state becomes

$$\frac{1}{\sqrt{2}} \left( |\uparrow\rangle_A \hat{a}^q |0_{2^m, \Theta}\rangle + |\downarrow\rangle_A \hat{a}^q |1_{2^m, \Theta}\rangle \right) \quad (12)$$

if  $q$  photons are lost. Here  $|\uparrow_A\rangle$  and  $|\downarrow_A\rangle$  represent the atomic state held by Alice. Analogously to the generation of this state, we also do the syndrome measurement with the help of a cavity. We adjust the cavity with the rotation angle  $\phi = \pi/2^{m-1}$  and the state of the atom inside is prepared to be  $(|\uparrow_s\rangle + |\downarrow_s\rangle) / \sqrt{2}$ . When we reflect the light mode after the transmission from this cavity, the joint atom–light state becomes

$$\begin{aligned} & \frac{1}{2} |\uparrow_s\rangle \left( |\uparrow_A\rangle \hat{a}^q |0_{2^m, \Theta}\rangle + |\downarrow_A\rangle \hat{a}^q |1_{2^m, \Theta}\rangle \right) \\ & + \frac{1}{2} |\downarrow_s\rangle \left( |\uparrow_A\rangle \hat{R}\left(\frac{\pi}{2^{m-1}}\right) \hat{a}^q |0_{2^m, \Theta}\rangle + |\downarrow_A\rangle \hat{R}\left(\frac{\pi}{2^{m-1}}\right) \hat{a}^q |1_{2^m, \Theta}\rangle \right), \end{aligned} \quad (13)$$

where  $|\uparrow_s\rangle$  and  $|\downarrow_s\rangle$  represent the state of the ancillary atom inside the cavity used for the syndrome measurement. There is a relation of the rotation operator  $\hat{R}(\phi)$  and the annihilation operator  $\hat{a}$

$$\begin{aligned} \hat{R}(\phi) \hat{a}^q &= \hat{R}(\phi) \hat{a}^q \hat{R}^\dagger(\phi) \hat{R}(\phi) = \left( \hat{R}(\phi) \hat{a} \hat{R}^\dagger(\phi) \right)^q \hat{R}(\phi) \\ &= \left( e^{-i\phi} \hat{a} \right)^q \hat{R}(\phi) = e^{-iq\phi} \hat{a}^q \hat{R}(\phi). \end{aligned} \quad (14)$$

Also, according to Equation (11), we have

$$\begin{aligned} \hat{R}\left(\frac{\pi}{2^{m-1}}\right) |0_{2^m, \Theta}\rangle &= |0_{2^m, \Theta}\rangle, \\ \hat{R}\left(\frac{\pi}{2^{m-1}}\right) |1_{2^m, \Theta}\rangle &= |1_{2^m, \Theta}\rangle. \end{aligned} \quad (15)$$

Then Equation (13) can be rewritten as

$$\frac{1}{2} \left( |\uparrow\rangle_s + e^{-\frac{iq\pi}{2^{m-1}}} |\downarrow\rangle_s \right) \left( |\uparrow\rangle_A \hat{a}^q |0_{2^m, \Theta}\rangle + |\downarrow\rangle_A \hat{a}^q |1_{2^m, \Theta}\rangle \right), \quad (16)$$

which is a product of the atomic state  $(|\uparrow\rangle_s + \exp(-iq\pi/2^{m-1})|\downarrow\rangle_s)/\sqrt{2}$  and the state in Equation (12). Thus, with the help of this kind of cavity, we can construct a quantum nondemolition measurement, which contains information in the atomic state of the syndrome spin about how many photons are lost from the light mode after transmission.

Unfortunately, there are also some constraints in such a scheme. First, the extra phase obtained in the atomic state  $\exp(-iq\pi/2^{m-1})$  is not unique for every  $q$  with finite  $m$ , e.g., for any  $q_1 \in N_0$ , if we choose  $q_2 = q_1 + 2^m$ , there is a relation  $\exp(-iq_2\pi/2^{m-1}) = \exp(-iq_1\pi/2^{m-1})$ . This means there can be states with uncorrectable errors, which cannot be distinguished by this method. This effect will decrease the total fidelity depending on the choice of the primitive state  $|\Theta\rangle$ . In Section 3, we will analyze in detail the performance of our repeater scheme for the special case of “cat codes”. Second, it is not always possible to deterministically discriminate the atomic states with different phases, even in theory, because in general they are not mutually orthogonal.<sup>[23,24]</sup> However, this complication can be circumvented by employing more cavities (or adjusting the same cavity many times). The idea is to extract partial information of  $q$  at several times and then combine all the partial information to get the full syndrome information. For this purpose, we first reflect the light mode in Equation (12) from a cavity with the rotation angle  $\phi = \pi$ . The resulting state is

$$\frac{1}{2} \left( |\uparrow\rangle_s + e^{-iq\pi} |\downarrow\rangle_s \right) \left( |\uparrow\rangle_A \hat{a}^q |0_{2^m, \Theta}\rangle + |\downarrow\rangle_A \hat{a}^q |1_{2^m, \Theta}\rangle \right), \quad (17)$$

where the extra phase  $e^{-iq\pi} = 1$  if  $q$  is even and  $e^{-iq\pi} = -1$  if  $q$  is odd. It is not difficult to discriminate the two orthogonal atomic states  $|\uparrow\rangle_s + |\downarrow\rangle_s$  and  $|\uparrow\rangle_s - |\downarrow\rangle_s$  and after the measurement of the atomic state, we have some information of  $q$ , i.e., whether it is even or odd. Next, we repeat this process but prepare the cavity with the rotation angle  $\phi = \pi/2$  and reflect the light mode again. Not surprisingly, this time the output state becomes<sup>[25]</sup>

$$\frac{1}{2} \left( |\uparrow\rangle_s + e^{-\frac{iq\pi}{2}} |\downarrow\rangle_s \right) \left( |\uparrow\rangle_A \hat{a}^q |0_{2^m, \Theta}\rangle + |\downarrow\rangle_A \hat{a}^q |1_{2^m, \Theta}\rangle \right). \quad (18)$$

Now we look at the cases when  $q$  is even or odd separately. In the case when  $q$  is even,  $e^{-iq\pi/2} = 1$  if  $q \bmod 4 = 0$ ,  $e^{-iq\pi/2} = -1$  if  $q \bmod 4 = 2$ . For the case that  $q$  is odd,  $e^{-iq\pi/2} = -i$  if  $q \bmod 4 = 1$ ,  $e^{-iq\pi/2} = i$  if  $q \bmod 4 = 3$ . In either case, the atomic states we need to discriminate are orthogonal (even: Pauli X eigenstates, odd: Pauli Y eigenstates). So in either case, the atomic states can be discriminated deterministically, at least in principle, by adapting the spin basis of the second measurement according to the outcome of the first (or by including a corresponding spin rotation prior to the second measurement depending on the result of the first). The steps above can be repeated again and again if we divide the rotation angle  $\phi$  in half at every step until  $\phi = \pi/2^{m-1}$  (see Section S1, Supporting Information). After all the steps, we will finally know the remainder of  $q$  divided

by  $2^m$ ,  $r_m(q)$ , i.e.,  $q \bmod 2^m = r_m(q)$ . The  $r_m(q)$  tells us which error space (or the code space) the light mode<sup>[7,8]</sup> and this is crucial to improve the total fidelity.

## 2.4. Entanglement Creation

In our protocol, the transmitted light mode is used to create the entanglement for the atomic states that Alice and Bob hold and the cavity-assisted method can also be used to create such entanglement. In order to do this, Bob needs to prepare another such cavity after his syndrome measurement and this time the rotation angle  $\phi$  should be  $\pi/2^m$ . With this angle, a “bit flip” happens after the corresponding rotation operator  $\hat{R}(\phi)$  acts on the two codewords in Equation (9), i.e.,

$$\begin{aligned} \hat{R}\left(\frac{\pi}{2^m}\right) |0_{2^m, \Theta}\rangle &= |1_{2^m, \Theta}\rangle, \\ \hat{R}\left(\frac{\pi}{2^m}\right) |1_{2^m, \Theta}\rangle &= |0_{2^m, \Theta}\rangle. \end{aligned} \quad (19)$$

These relations can be derived from Equation (10) using  $\hat{R}(\phi)\hat{R}(\psi) = \hat{R}(\phi + \psi)$  with any arbitrary  $\phi$  and  $\psi$ . Thus, the state after this interaction becomes (using again Equation (14) and now, in addition, Equation (19))

$$\begin{aligned} &\frac{1}{2} |\uparrow\rangle_B \left( |\uparrow\rangle_A \hat{a}^q |0_{2^m, \Theta}\rangle + |\downarrow\rangle_A \hat{a}^q |1_{2^m, \Theta}\rangle \right) \\ &+ \frac{1}{2} e^{-\frac{iq\pi}{2^m}} |\downarrow\rangle_B \left( |\uparrow\rangle_A \hat{a}^q |1_{2^m, \Theta}\rangle + |\downarrow\rangle_A \hat{a}^q |0_{2^m, \Theta}\rangle \right) \\ &= \frac{1}{2} \left[ \left( |\uparrow\rangle_B |\uparrow\rangle_A + e^{-\frac{iq\pi}{2^m}} |\downarrow\rangle_B |\downarrow\rangle_A \right) \hat{a}^q |0_{2^m, \Theta}\rangle \right. \\ &\quad \left. + \left( |\uparrow\rangle_B |\downarrow\rangle_A + e^{-\frac{iq\pi}{2^m}} |\downarrow\rangle_B |\uparrow\rangle_A \right) \hat{a}^q |1_{2^m, \Theta}\rangle \right]. \end{aligned} \quad (20)$$

Because this interaction happens after the syndrome measurement,  $r_m(q)$  is supposed to be known. Finally, according to Equation (20), the discrimination between the light states  $\hat{a}^q |0_{2^m, \Theta}\rangle$  and  $\hat{a}^q |1_{2^m, \Theta}\rangle$  (actually, the states to be discriminated are not exactly these two states if the full loss channel is considered, as we shall discuss in Section 3.4 in more detail) leads to a collapse for the state in Equation (20) and the conditional atomic state of Alice and Bob will always become entangled. However,  $\hat{a}^q |0_{2^m, \Theta}\rangle$  and  $\hat{a}^q |1_{2^m, \Theta}\rangle$  are generally not orthogonal, thus the discrimination cannot be done deterministically (or otherwise in an error-free fashion). This is the only nondeterministic element in our scheme if we choose an error-free, unambiguous discrimination. There are several ways to do the state discrimination, with distinct advantages and drawbacks. A detailed discussion will be presented in Section 3. The final entangled state will be either  $|\uparrow\rangle_B |\uparrow\rangle_A + \exp(-iq\pi/2^m) |\downarrow\rangle_B |\downarrow\rangle_A$  or  $|\uparrow\rangle_B |\downarrow\rangle_A + \exp(-iq\pi/2^m) |\downarrow\rangle_B |\uparrow\rangle_A$ , depending on the measurement result for the light mode. Again note that  $q$  is assumed to be known, so we have full information of the final entangled state, which means this kind of entanglement can be a resource for quantum communication. An error in measuring  $q$  would eventually result in reduced atomic state fidelities. In principle, however, the

$q$  identification is quite reliable, as it is based on an orthogonal projection measurement of the syndrome spins.

### 2.5. Full Loss Channel

All the discussions in Sections 2.3 and 2.4 are based on the simplified loss channel, but in practice, photon loss is described by the full, physical amplitude damping (AD) channel.<sup>[7,26]</sup> Generally, a single-mode state after the action of AD is mixed and it can be expressed as

$$\hat{\rho}' = \sum_{k=0}^{\infty} \hat{A}_k \hat{\rho} \hat{A}_k^\dagger, \quad (21)$$

where  $\hat{\rho}$  and  $\hat{\rho}'$  are the density operators of the states before and after the action of the channel, respectively. Here,  $\hat{A}_k$  is a nonunitary error operator<sup>[7,26]</sup>

$$\begin{aligned} \hat{A}_k &= \sum_{n=k}^{\infty} \sqrt{\binom{n}{k}} \sqrt{\eta^{n-k} (1-\eta)^k} |n-k\rangle \langle n| \\ &= \sqrt{\frac{(1-\eta)^k}{k!}} \sqrt{\eta}^{\hat{n}} \hat{a}^k, \quad \forall k \in \mathbb{N}_0, \end{aligned} \quad (22)$$

where  $\eta$  is the transmission of the fiber, i.e., the probability of losing one photon is  $1 - \eta$ .

Then the action of AD on the state in Equation (9) leads to a mixed state and the final density operator becomes

$$\hat{\rho}_f = \sum_{k=0}^{\infty} \hat{A}_k \frac{1}{\sqrt{2}} (|\uparrow\rangle|0_{2^m, \Theta}\rangle + |\downarrow\rangle|1_{2^m, \Theta}\rangle) \times \text{H.c.} \quad (23)$$

Next, if there is a rotation operator acting on it, the density operator transforms as

$$\begin{aligned} \hat{R}(\phi) \hat{\rho}_f \hat{R}^\dagger(\phi) &= \sum_{k=0}^{\infty} \hat{R}(\phi) \hat{A}_k \frac{1}{\sqrt{2}} (|\uparrow\rangle|0_{2^m, \Theta}\rangle + |\downarrow\rangle|1_{2^m, \Theta}\rangle) \\ &\quad \times \text{H.c.} \end{aligned} \quad (24)$$

If we only look at the  $k$ -component of Equation (24) and temporarily ignore the Hermitian conjugate (H.c.) of it, i.e.,

$$\begin{aligned} &\hat{R}(\phi) \hat{A}_k \frac{1}{\sqrt{2}} (|\uparrow\rangle|0_{2^m, \Theta}\rangle + |\downarrow\rangle|1_{2^m, \Theta}\rangle) \\ &= e^{i\phi\hat{n}} \sqrt{\frac{(1-\eta)^k}{k!}} \sqrt{\eta}^{\hat{n}} \hat{a}^k \frac{1}{\sqrt{2}} (|\uparrow\rangle|0_{2^m, \Theta}\rangle + |\downarrow\rangle|1_{2^m, \Theta}\rangle) \\ &= \left( \sqrt{\frac{(1-\eta)^k}{k!}} \sqrt{\eta}^{\hat{n}} \right) e^{i\phi\hat{n}} \hat{a}^k \frac{1}{\sqrt{2}} (|\uparrow\rangle|0_{2^m, \Theta}\rangle + |\downarrow\rangle|1_{2^m, \Theta}\rangle). \\ &= e^{-ik\phi} \left( \sqrt{\frac{(1-\eta)^k}{k!}} \sqrt{\eta}^{\hat{n}} \hat{a}^k \right) e^{i\phi\hat{n}} \frac{1}{\sqrt{2}} (|\uparrow\rangle|0_{2^m, \Theta}\rangle + |\downarrow\rangle|1_{2^m, \Theta}\rangle) \\ &= e^{-ik\phi} \frac{1}{\sqrt{2}} (|\uparrow\rangle \hat{A}_k \hat{R}(\phi) |0_{2^m, \Theta}\rangle + |\downarrow\rangle \hat{A}_k \hat{R}(\phi) |1_{2^m, \Theta}\rangle). \end{aligned} \quad (25)$$

Comparing Equation (25) with Equation (16), including the steps for the syndrome detection in Equations (13)–(16), it is obvious that for the  $k$ - or  $q$ -components, the only difference is that  $\hat{a}^k$  is replaced by  $\hat{A}_k$ , bringing a prefactor  $\hat{A}_k / \hat{a}^k = \sqrt{(1-\eta)^k / k!} \sqrt{\eta}^{\hat{n}}$ . Thus, all the results in Sections 2.3 and 2.4 are exactly applicable for the full loss channel up to these prefactors acting on each component. It is not straightforward what effects these prefactors will bring for an arbitrary primitive state  $|\Theta\rangle$ . As an example of our scheme, we refer to a part of the results given by Bergmann and van Loock<sup>[7]</sup> and evaluate the performance of our repeater protocol using the “cat codes”.

## 3. Analysis

In the preceding section, we describe the basic elements of our protocol that could be used, in principle, for quantum communication over long distances at high rates. Here in this section, we explicitly propose such a scheme for long-distance quantum communication based on these elements. We will evaluate the performance of this scheme numerically for a particular case of the rotation-symmetric bosonic codes—the cat codes.

### 3.1. Scheme for Long-Distance Quantum Communication

We want to propose a scheme without the need of quantum memories, similar to a third-generation quantum repeater,<sup>[4]</sup> with the goal not to slow down the repeater due to two-way classical communication and the corresponding waiting times. But instead of directly transmitting encoded qubits, in our scheme, we aim to create entangled states shared between Alice and Bob over a long distance.

Realizing long-distance quantum communication directly from one point (Alice) to another (Bob) connected by a fiber channel is not efficient because of the photon loss in the fiber, and so intermediate stations have to be employed along the channel between Alice and Bob in order to suppress the exponential decay of either qubit rates or qubit state fidelities. Assume that the total distance between Alice and Bob is  $L_{\text{tot}}$ , then the repeater stations are placed at every elementary distance  $L_0 = L_{\text{tot}} / n_e$ , where  $n_e$  is the number of elementary links. The repeater stations are divided into two different types according to their function: one is for sending the light and the other one is for receiving it (see **Figure 2**).

The structure of the two kinds of elementary stations is depicted in **Figure 3**.  $ES_1$ , which sends the light, consists of two cavities. The cavities are used to generate the desired light mode state according to Section 2.2 and the two modes just generated are then sent to the two nearest stations separately in opposite directions. For  $ES_2$ , which receives the light, the number of involved cavities varies depending on the loss order of the code. The syndrome measurements and the entanglement creation are performed in  $ES_2$  as described in Sections 2.3 and 2.4. Note that the number of cavities needed in each repeater station can be different from what is depicted in **Figure 3**, because for the generation and the syndrome measurement procedures, one can either use one cavity many times with different parameters or use many different cavities only once. It is obvious that



**Figure 2.** Schematic of the long-distance entanglement distribution protocol including two types of elementary stations:  $ES_1$  to send the light mode and  $ES_2$  to receive it.

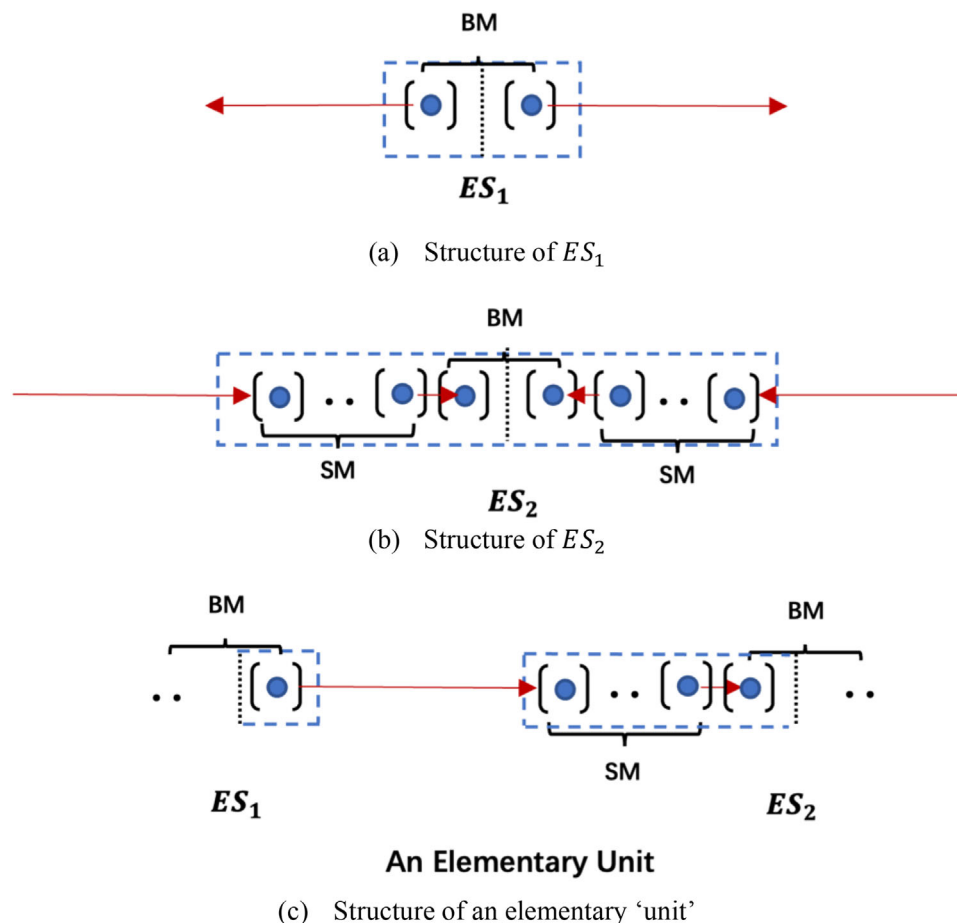


**Figure 3.** The structure of two types of elementary stations: a)  $ES_1$  and b)  $ES_2$ , c) one half of  $ES_1$  and one half of  $ES_2$  together can form an elementary “unit”. The different spin measurements are denoted by BM (Bell measurement) and SM (syndrome measurement).

$ES_1$  and  $ES_2$  are mirror-symmetric, so both can be divided into two parts. The right part of  $ES_1$  and the left part of  $ES_2$  (or the other way around) can form a basic elementary unit of the whole protocol. In an elementary unit, all the three procedures including state preparation, syndrome measurement, and entanglement creation are performed in corresponding order. This results in an entangled state between the atomic spin in  $ES_1$  and the atom inside the last cavity that interacted with the light mode in  $ES_2$ . Thus, many such elementary units connecting each other can form the whole repeater protocol. Bell measurements are then performed on the two still unmeasured spins at every repeater station to swap the entanglement and hence coherently connect the individual segments. Finally, the atomic spins in Alice’s and Bob’s hands are entangled over the total distance (at least “effectively” entangled in case Alice and Bob decide to

measure their qubits immediately depending on the repeater’s application).

In practice, the Bell measurement on the two atoms at every  $ES_1$  can be done directly after the state preparation process. This way the entanglement between the atoms in every half of  $ES_1$  and the corresponding light mode sent away becomes the entanglement between the two light modes that  $ES_1$  has sent. So, there is no need to use quantum memories at  $ES_1$  to store the light entanglement (but memories may still be employed by Alice and Bob if they want to keep their entangled pairs). The sender and receiver stations (of Alice and Bob) do not constitute a complete  $ES_1$  or  $ES_2$ , but only a half of it. At each  $ES_1$  which connects two nearest “units”, the state preparation at the two parts must finish at the same time and the Bell measurement will be done immediately after the state preparation (so now the two flying light modes get



entangled). We assume that all the elementary distances between two nearest stations are the same. Then the light modes will arrive at every  $ES_2$  simultaneously, followed by the syndrome measurement and the entanglement creation. After all the processes, the atoms at the  $ES_2$  parts in the nearest “units” connected by  $ES_1$  get entangled. Finally, after doing Bell measurements at all the  $ES_2$ 's, the atomic states in Alice's and Bob's hands are entangled. More details of the derivations can be found in Section S7 of the Supporting Information. Also, if we do not need to keep the entangled pairs for Alice and Bob, e.g., when doing QKD, Alice and Bob can measure their atoms immediately and do not need the memories either. In conclusion, as long as all the events are sufficiently well synchronized, no quantum memories are needed in the whole scheme to realize long-distance quantum communication. The precise moment when we do the Bell measurements at the  $ES_1$ 's is irrelevant to the final joint state for Alice and Bob, so for simplicity and without loss of generality, the related theoretical derivations are mostly based on what happens in a single elementary “unit”.

For every elementary unit, there is a nonunit fidelity  $F_0$  for the distributed spin-spin entangled states and a nonunit success probability  $P_0$  for the state discrimination used to create the entanglement. The total success probability  $P_{\text{tot}}$  is the probability that the state discrimination succeeds at every station, so it is easy to get the relation,  $P_{\text{tot}} = P_0^{N_e}$ . To calculate the total fidelity  $F_{\text{tot}}$ , it is necessary to consider the entanglement swapping process (also see Section S4, Supporting Information).<sup>[27,28]</sup>

### 3.2. Cat Codes

As described in Section 2.2, for any optical states, it is possible to construct a so-called RSBC as in Equation (10). The “cat codes” are a special case for the RSBC, for which we choose the primitive state  $|\Theta\rangle$  to be the optical coherent state  $|\alpha\rangle = \exp(-|\alpha|^2/2) \sum_{n=0}^{\infty} \alpha^n |n\rangle/n!$ , where  $|n\rangle$  is the photon number state with photon number equal to  $n$ .<sup>[5,7,29]</sup> The amplitude  $\alpha$  is an important parameter in our scheme and it must be precisely controlled via the corresponding laser intensity (and so the average photon number  $|\alpha|^2$ ). Thus, the corresponding codewords are<sup>[7]</sup>

$$\begin{aligned} |0_{M,\text{cat}}\rangle &= \frac{1}{\sqrt{N_M}} \sum_{k=0}^{M-1} \hat{R}\left(\frac{2k\pi}{M}\right) |\alpha\rangle = \frac{1}{\sqrt{N_M}} \sum_{k=0}^{M-1} \left| \alpha e^{\frac{2k\pi i}{M}} \right\rangle, \\ |1_{M,\text{cat}}\rangle &= \frac{1}{\sqrt{N_M}} \sum_{k=0}^{M-1} \hat{R}\left(\frac{(2k+1)\pi}{M}\right) |\alpha\rangle \\ &= \frac{1}{\sqrt{N_M}} \sum_{k=0}^{M-1} \left| \alpha e^{\frac{(2k+1)\pi i}{M}} \right\rangle. \end{aligned} \quad (26)$$

It is then straightforward to find out the cyclic behavior for cat codes in the simplified loss model<sup>[7]</sup>

$$\begin{aligned} \hat{a}^{Mn} |0_{M,\text{cat}}\rangle &= \alpha^{Mn} |0_{M,\text{cat}}\rangle, \\ \hat{a}^{Mn} |1_{M,\text{cat}}\rangle &= (-1)^n \alpha^{Mn} |1_{M,\text{cat}}\rangle, \end{aligned} \quad (27)$$

$\forall n \in N_0$ . The cyclic rule means that for cat codes, the codewords or the states in an error space will come back to the corresponding

code or error space, which contributes to the total fidelity. Recall that the method in Section 2.2 can only generate states with  $M = 2^m$ .

After some lengthy calculations,<sup>[7]</sup> the density matrix of the joint state of the atom (at Alice again considering first a single link between Alice and Bob) and the light mode after the LBC becomes

$$\hat{\rho} = \sum_{q=0}^{2^{m+1}-1} p_q \left( \frac{|\uparrow\rangle_A \hat{a}^q |\tilde{0}_{2^m,\text{cat}}\rangle + |\downarrow\rangle_A \hat{a}^q |\tilde{1}_{2^m,\text{cat}}\rangle}{\sqrt{2N'_{m,q}}} \right) \times \text{H.c.} \quad (28)$$

where the statistical weights are (assuming real  $\alpha$ )

$$p_q = \frac{1}{\sqrt{N'_M}} \sum_{j=0}^{\infty} \frac{[\alpha^2(1-\eta)]^{2^{m+1}j+q}}{(2^{m+1} \cdot j + q)!}. \quad (29)$$

Here,  $|\tilde{0}_{2^m,\text{cat}}\rangle$  and  $|\tilde{1}_{2^m,\text{cat}}\rangle$  are the damped codewords

$$\begin{aligned} |\tilde{0}_{2^m,\text{cat}}\rangle &= \frac{1}{\sqrt{N'_M}} \sum_{k=0}^{M-1} \hat{R}\left(\frac{2k\pi}{M}\right) |\sqrt{\eta}\alpha\rangle, \\ |\tilde{1}_{2^m,\text{cat}}\rangle &= \frac{1}{\sqrt{N'_M}} \sum_{k=0}^{M-1} \hat{R}\left(\frac{(2k+1)\pi}{M}\right) |\sqrt{\eta}\alpha\rangle, \end{aligned} \quad (30)$$

which means the amplitudes of the coherent-state components are damped. The states in loss space— $\hat{a}^q |\tilde{0}_{2^m,\text{cat}}\rangle$  and  $\hat{a}^q |\tilde{1}_{2^m,\text{cat}}\rangle$ —are not normalized anymore, so a normalization constant  $N'_{m,q}$  is needed to normalize them ( $\hat{a}^q |\tilde{0}_{2^m,\text{cat}}\rangle / \sqrt{N'_{m,q}}$  and  $\hat{a}^q |\tilde{1}_{2^m,\text{cat}}\rangle / \sqrt{N'_{m,q}}$  are normalized states now). Because of the cyclic behavior presented in Equation (27), all the terms with  $q \geq 2^{m+1}$  have their corresponding terms with  $q < 2^{m+1}$  and they can be simply added up. The terms of Equation (28) can be divided into two parts—the first  $2^m$  terms and the last  $2^m$  terms. According to Section 2.3, the first  $2^m$  terms can be individually distinguished in a deterministic fashion and the last  $2^m$  terms are uncorrectable errors. So, after the syndrome measurement, the density matrix will collapse to

$$\begin{aligned} \hat{\rho}'' &= \frac{p_q}{p_q + p_{q+2^m}} \left( \frac{|\uparrow\rangle_A \hat{a}^q |\tilde{0}_{2^m,\text{cat}}\rangle + |\downarrow\rangle_A \hat{a}^q |\tilde{1}_{2^m,\text{cat}}\rangle}{\sqrt{2NM, q'}} \right) \times \text{H.c.} \\ &+ \frac{p_{q+2^m}}{p_q + p_{q+2^m}} \left( \frac{|\uparrow\rangle_A \hat{a}^q |\tilde{0}_{2^m,\text{cat}}\rangle - |\downarrow\rangle_A \hat{a}^q |\tilde{1}_{2^m,\text{cat}}\rangle}{\sqrt{2N'M, q}} \right) \times \text{H.c.}, \end{aligned} \quad (31)$$

with probability  $p_q + p_{q+2^m}$ , which depends on the result of the measurement of the atomic state (here  $q < 2^m$  and we make use of the cyclic behavior). According to Section 2.4, after another cavity reflection, the state becomes

$$\hat{\rho}''' = \frac{p_q}{p_q + p_{q+2^m}} \left( \frac{|\Phi_{q\pi/2^m}^+\rangle_{BA} \hat{a}^q |\tilde{0}_{2^m, cat}\rangle + |\Psi_{q\pi/2^m}^+\rangle_{BA} \hat{a}^q |\tilde{1}_{2^m, cat}\rangle}{\sqrt{2N_{M,q'}}} \right) \times \text{H.c.} \quad (32)$$

$$+ \frac{p_{q+2^m}}{p_q + p_{q+2^m}} \left( \frac{|\Phi_{q\pi/2^m}^-\rangle_{BA} \hat{a}^q |\tilde{0}_{2^m, cat}\rangle + |\Psi_{q\pi/2^m}^-\rangle_{BA} \hat{a}^q |\tilde{1}_{2^m, cat}\rangle}{\sqrt{2N_{M,q'}}} \right) \times \text{H.c.},$$

where  $|\Phi_{\pm}^{q\pi/2^m}\rangle_{BA}$  and  $|\Psi_{\pm}^{q\pi/2^m}\rangle_{BA}$  are the generalizations of the four Bell states. These are defined as

$$|\Phi_{\theta}^{\pm}\rangle_{BA} = \frac{|\uparrow\rangle_B |\uparrow\rangle_A \pm e^{-i\theta} |\downarrow\rangle_B |\downarrow\rangle_A}{\sqrt{2}}, \quad (33)$$

$$|\Psi_{\theta}^{\pm}\rangle_{BA} = \frac{|\uparrow\rangle_B |\downarrow\rangle_A \pm e^{-i\theta} |\downarrow\rangle_B |\uparrow\rangle_A}{\sqrt{2}}.$$

Then after the state discrimination for the light mode, the final atomic state shared by Alice and Bob (i.e., here, in a single repeater segment) becomes a mixture of  $|\Phi_{+}^{q\pi/2^m}\rangle_{BA}$  and  $|\Phi_{-}^{q\pi/2^m}\rangle_{BA}$  or a mixture of  $|\Psi_{+}^{q\pi/2^m}\rangle_{BA}$  and  $|\Psi_{-}^{q\pi/2^m}\rangle_{BA}$  depending on the results of the state discrimination. In this case, our target is the state  $|\Phi_{+}^{q\pi/2^m}\rangle_{BA}$  or  $|\Psi_{+}^{q\pi/2^m}\rangle_{BA}$ . Because  $|\Phi_{+}^{q\pi/2^m}\rangle_{BA}$  (or  $|\Psi_{+}^{q\pi/2^m}\rangle_{BA}$ ) and  $|\Phi_{-}^{q\pi/2^m}\rangle_{BA}$  (or  $|\Psi_{-}^{q\pi/2^m}\rangle_{BA}$ ) are orthogonal, the  $(q + 2^m)$ -terms have no contribution to the total fidelity. Finally, we obtain the fidelity in an elementary, entangled-state distribution unit (i.e., the initial fidelity in a loss-corrected repeater segment)

$$F_0 = \sum_{q=0}^{2^m-1} p_q, \quad (34)$$

which is the sum of the statistical weights of the first  $2^m$  terms of  $\hat{\rho}'$ .

Typically, there are two choices for the discrimination of light-mode quantum states, homodyne measurement or USD based on photon measurements, and these have distinct properties. The case with homodyne measurement can be deterministic or probabilistic depending on how one defines a successful measurement outcome, but the fidelity will typically decrease with growing success probability. The USD does not affect the fidelity (i.e., it is error-free), but it cannot be done deterministically for nonorthogonal states. Also, for larger loss orders ( $L > 1$ ), it is subtle to define a successful measurement in a suitable manner. In our model, USD seems more appropriate, even though it cannot be done deterministically. The maximal success probability for USD is<sup>[23,24]</sup>

$$\max P_{\text{USD}} = 1 - |\langle \psi_1 | \psi_2 \rangle|, \quad (35)$$

where  $|\psi_1\rangle$  and  $|\psi_2\rangle$  are the states to be distinguished with equal a priori probabilities. In our case, the maximal success probability

to do USD in an elementary unit is then

$$\max P_0 = 1 - |\langle \tilde{0}_{2^m, \Theta}^q | \tilde{1}_{2^m, \Theta}^q \rangle|. \quad (36)$$

Since in our case,  $|\tilde{0}_{2^m, \Theta}^q\rangle$  and  $|\tilde{1}_{2^m, \Theta}^q\rangle$  are not orthogonal, the maximal success probability is certainly below one for finite  $\alpha$ . However, provided  $\alpha$  is sufficiently large, the overlap will almost vanish and then the probability can be close to unity. In this case though, with growing  $\alpha$ , the photon loss (hence, in Equation (32), the uncorrectable phase-flip) probability increases.

### 3.3. Numerical Analysis Based on Cat Codes

According to Section 3.2, it is obvious that the fidelity and the success probability in an elementary unit,  $F_0$  and  $P_0$ , depend on the elementary distance  $L_0$ . Generally, to get near-unit  $F_0$  and  $P_0$ ,  $L_0$  needs to be rather small, but a small  $L_0$  leads to a big  $n_e$  (at a given total distance), which occurs in the powers for the total fidelity and success probability, and eventually again decreases them. So, there is a trade-off concerning the choice of the elementary distance, but this is closely related to the choice of how to encode the information. Fortunately, in our setting, this relation is rather simple—both the total fidelity and the total success probability improve with decreasing  $L_0$  (see **Figure 4**). However, in practice, having too many stations means a high experimental cost, which is undesirable. Moreover, the local experimental imperfections, especially cavity loss and more generally any form of coupling losses (see below), contribute to a greater extent for an increasing number of stations. Thus, the stations need to be as few as possible and, at the same time,  $F_{\text{tot}}$  and  $P_{\text{tot}}$  should be near unity.

For fixed  $L_0$  and  $L_{\text{tot}}$ ,  $F_{\text{tot}}$ , and  $P_{\text{tot}}$  also depend on the amplitude  $\alpha$  in the two codewords. Here is again a trade-off—for too large  $\alpha$ , photons are more likely to get lost (with increased weights of the uncorrectable loss terms) and hence  $F_{\text{tot}}$  decreases, while the two codewords become more orthogonal and hence the success probability for the state discrimination increases. Conversely, for smaller  $\alpha$ ,  $F_{\text{tot}}$  becomes larger and  $P_{\text{tot}}$  becomes smaller. A larger loss order  $L = 2^m - 1$  is also beneficial for the fidelity, but it leads to a decreasing  $P_{\text{tot}}$ . As shown in Figure 4, for repeaterless cases ( $L_0 = L_{\text{tot}} = 1000$  km), the fidelities do not always go down with increasing  $\alpha$ . This can be explained by looking at what happens when  $\alpha$  increases from zero. For example, for the 1-loss code ( $L = 1$ ), when  $\alpha$  is very small, it is most probable to lose zero or one photons, in which case we would be able to correct the codewords. When  $\alpha$  becomes larger, the probability to lose two

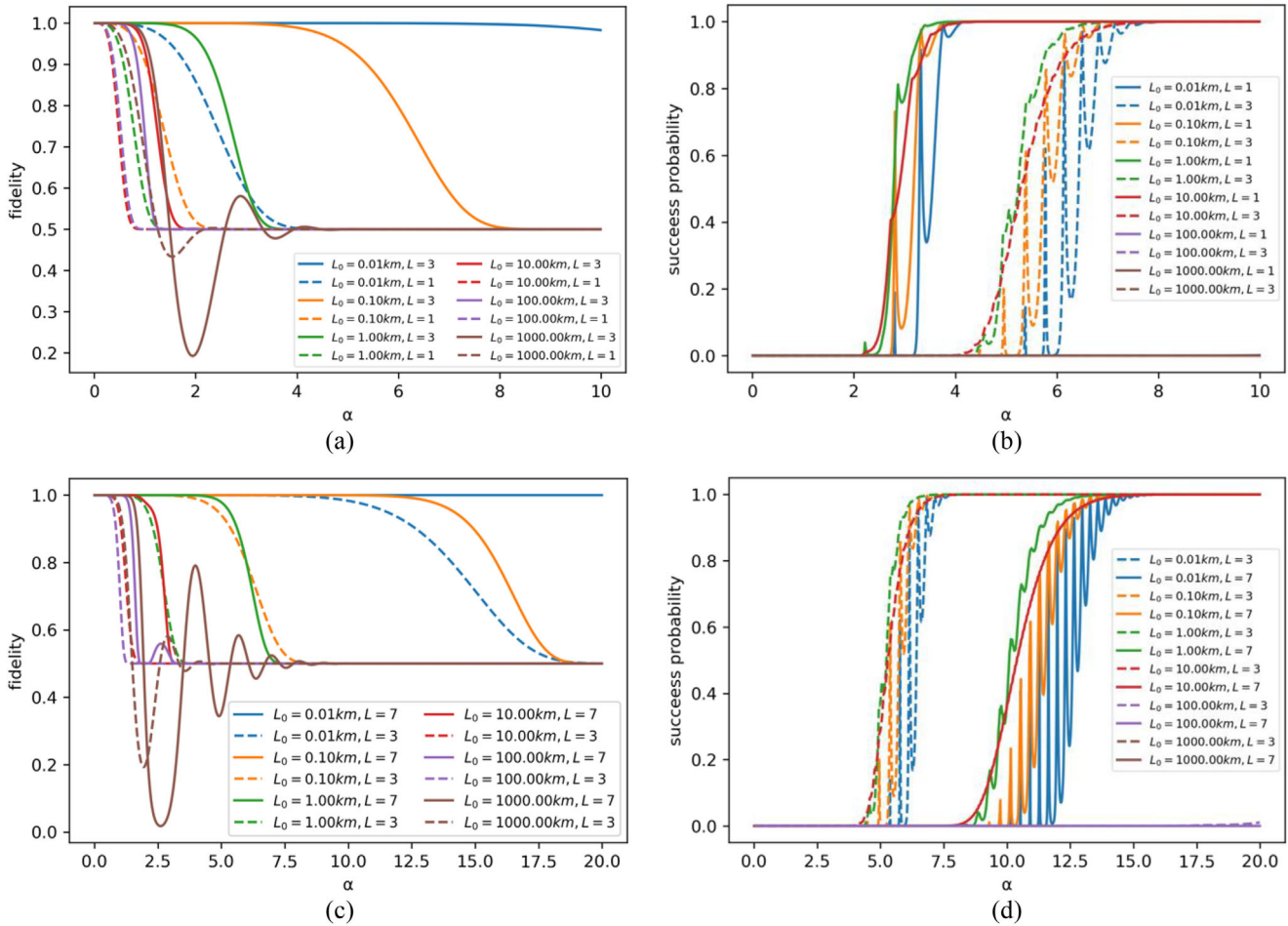


**Figure 4.** a,c) The total fidelity  $F_{\text{tot}}$  and b,d) the total success probability  $P_{\text{tot}}$  as a function of  $\alpha$  for various elementary distances  $L_0$ :  $L_0 = 0.01$  km (blue),  $L_0 = 0.1$  km (orange),  $L_0 = 1$  km (green),  $L_0 = 10$  km (red),  $L_0 = 100$  km (purple), and  $L_0 = 1000$  km (brown). We compare them for the 1-loss (dashed) and 3-loss (solid) codes in (a) and (b) and for the 3-loss (dashed) and 7-loss (solid) codes in (c) and (d). The total distance is always chosen to be 1000 km. Here and in the subsequent figures, the parameter  $\alpha$  corresponds to the real-valued amplitude of the coherent states as employed in our cavity-QED-based scheme where  $\alpha^2$  is the average photon number.

or three photons, contributing to the set of uncorrectable errors, increases, and at some point, the weights of the corresponding terms will dominate in the density operator, so the fidelity will then drop. However, if  $\alpha$  keeps increasing, then the probability to lose four or five photons will also increase and start contributing. This time, because we can correct the errors coming from four and five photon losses, the fidelities will go up again. The situation is similar when  $\alpha$  becomes even larger and so the fidelities will oscillate, going up and down. For the case when the repeater stations are included, we also have to include the entanglement swapping operations. According to Section 3.1,  $n_e$  (the number of elementary “units”) is always even (10, 100, 1000...) except when  $L_0 = 1000$  km ( $n_e = 1$  in this case), and then according to Equation (S21) of the Supporting Information, the fidelities can no longer go below 1/2.

To summarize, we need to determine an  $\alpha$ -regime which allows for near-unit  $F_{\text{tot}}$  and  $P_{\text{tot}}$  with  $L_0$  being as large as possible. As shown in Figure 4a,b, for the 1-loss cat code, this kind of  $\alpha$  regime does not exist with  $L_0 \geq 0.01$  km, which means more than a hundred thousand stations are needed for a total distance

of 1000 km. Obviously, it is then not an optimal choice to use the 1-loss cat code. Fortunately, if we consider codes, there is such an  $\alpha$  regime with a suitable choice of  $L_0$ . The behaviors of  $F_{\text{tot}}$  and  $P_{\text{tot}}$  based on the 3-loss and 7-loss codes are shown in Figure 4c,d. For the 3-loss code, the appropriate  $\alpha$  regime does exist, with  $L_0 \approx 0.01$  km, and for the 7-loss code, it works with  $L_0 \approx 0.1$  km. Thus, one may expect that there is such a suitable  $\alpha$  regime for even larger  $L_0$  if the loss order goes beyond seven (while  $L_0$  must remain sufficiently small; clearly smaller than 15 km which corresponds to a channel transmission of at least 1/2 per segment).

### 3.4. Secret Key Rate Analysis

An important possible application of entanglement distribution is QKD. Our repeater protocol, in principle, can then be used for long-range QKD. According to Section 3.2 (also see Section S4, Supporting Information), one possibility for the final quantum state (shared among Alice and Bob) is presented in

Equation (S16) of the Supporting Information. Here we rewrite it as

$$\left( \frac{1}{2} + \frac{1}{2} \prod_{i=0}^{2^m-1} \left( \frac{p_i - p_{i+2^m}}{p_i + p_{i+2^m}} \right)^{t_i} \right) |\Phi_{q\pi/2^m}^+\rangle \langle \Phi_{q\pi/2^m}^+| + \left( \frac{1}{2} - \frac{1}{2} \prod_{i=0}^{2^m-1} \left( \frac{p_i - p_{i+2^m}}{p_i + p_{i+2^m}} \right)^{t_i} \right) |\Phi_{q\pi/2^m}^-\rangle \langle \Phi_{q\pi/2^m}^-|, \quad (37)$$

with a corresponding success probability as described in Equation (S20) of the Supporting Information. Note here that  $|\Phi_{q\pi/2^m}^\pm\rangle$  can also be replaced by  $|\Psi_{q\pi/2^m}^\pm\rangle$  depending on all the results of the Bell measurements being done in the entanglement swapping process. If we define the fidelity in this case as  $F_{\{t_i\}}$ , then Equation (37) can be rewritten as

$$F_{\{t_i\}} \left( |\Phi_{q\pi/2^m}^+\rangle \langle \Phi_{q\pi/2^m}^+| + (1 - F_{\{t_i\}}) |\Phi_{q\pi/2^m}^-\rangle \langle \Phi_{q\pi/2^m}^-| \right), \quad (38)$$

The (asymptotic) secret key rate is the product of the raw rate and the secret key fraction<sup>[30]</sup>

$$R_{\text{QKD}} := R_{\text{raw}} r_{\infty}. \quad (39)$$

The raw rate  $R_{\text{raw}}$  in our case is

$$R_{\text{raw}} = \frac{1}{t_0} P_{\text{tot}}, \quad (40)$$

where  $t_0 \approx 10^{-6}$  s is the typical repetition time when light–matter interfaces and couplings are involved, which corresponds to an experimental clock rate  $\sim$  MHz (recall that our scheme is memoryless and hence independent of the usual waiting times for classical signals in memory-based quantum repeater schemes; unlike all-photonic quantum repeaters, however, clock rates  $\sim$  GHz will be hard to achieve in our case). In our scheme, when employed for QKD, Alice and Bob can measure their atomic states immediately and the complete classical information about the Bell measurement outcomes from the entanglement swapping at all the repeater stations can be transferred to them at the end with no need to wait for any classical signals at an earlier stage. Thus, the raw rates have no fundamental limitation in theory and here we just choose a typical repetition time in the lab in order to analyze the secret key rates. We consider an entanglement-based version of the BB84 scheme. The BB84 secret key fraction is given by<sup>[28,30]</sup>

$$r_{\infty}^{\text{BB84}} = 1 - h(e_X) - h(e_Z), \quad (41)$$

where  $h(p)$  is the binary entropy function and  $e_{X/Z}$  are the quantum bit error rates (QBERs). For the explicit state in Equations (37) and (38), the averaged QBERs  $e_X$  and  $e_Z$  are<sup>[28,30]</sup>

$$e_X = 1 - F_{\{t_i\}}, \quad e_Z = 0. \quad (42)$$

After some additional derivations (see Section S5, Supporting Information), we get a lower bound of the averaged secret fraction for the BB84 protocol, which can be written as

$$r_{\infty}^{\text{BB84}} > 1 - h(F_{\text{tot}}). \quad (43)$$

Hence the lower bound of the secret key rate  $R_{\text{LB}}$  is given by

$$R_{\text{QKD}} > R_{\text{LB}} = \frac{1}{t_0} P_{\text{tot}} (1 - h(F_{\text{tot}})), \quad (44)$$

where  $R_{\text{QKD}}$  is the secret key rate for the QKD system.

The secret key rate incorporates both the fidelity and the success probability. As shown in Figure 5a,b, for the 1-loss code, if the elementary distance is 0.01 km, it is possible to get a nonzero secret key rate, but in a rather narrow range of  $\alpha$  (total distance: 1000 km). If the elementary distance is equal to 0.1 km, the secret key rate is always zero. This is similar to what we discussed in Section 3.3—for  $L = 1$ , there is no such  $\alpha$ -regime that both  $F_{\text{tot}}$  and  $P_{\text{tot}}$  are large enough. Analogously, for  $L = 3$  and  $L = 7$ , the secret key rate can be nonzero for an elementary distance of 0.01 and 0.1 km, but this requires larger  $\alpha$ . It can be seen from Figure 5b,d,f that the secret key rate per channel use  $R_{\text{QKD}} t_0$  is much smaller than one with an elementary distance of 0.01 km for the 1-loss code. However, it can be very close to unity for the 3-loss code with an elementary distance of 0.01 km, and in this case, it can also be nonzero with an elementary distance of 0.1 km, but the rate is still not very large in this case. For the 7-loss code, it can be close to unity even with an elementary distance of 0.1 km. Therefore, it is reasonable to suppose that for higher-loss codes ( $L > 7$ ), the secret key rate can be nonzero with larger elementary distances and the secret key rate per channel use may even reach unity with a large enough elementary distance (e.g.,  $L_0 = 0.1$  km or even larger).

Here, the total distance is always  $L_{\text{tot}} = 1000$  km and the corresponding (repeaterless) total transmittance is  $\eta_{\text{tot}} = \exp(-L_{\text{tot}}/L_{\text{att}}) \approx 1.82 \times 10^{-20}$ , so for the corresponding PLOB bound we have,<sup>[31,32]</sup>  $-\log_2(1 - \eta_{\text{tot}}) \approx \eta_{\text{tot}} / \ln(2) \approx 2.62 \times 10^{-20}$ . Then, as it can be seen in Figure 5, the secret key rates per channel use can significantly exceed the PLOB bound with loss orders  $L = 1, 3, 7$  and suitably chosen values for  $\alpha$ .

Besides channel loss, in a real experiment, there are also errors caused by the local imperfections such as the photon loss related with the cavity interfaces at every repeater station as well as imperfect measurements. What we discussed in Section 2.5 is also applicable for the local photon loss, but the corresponding transmission parameter  $\eta$  will depend on the cavities and the way to do the measurements (instead of the channel distance). Since the local errors will accumulate at every station, more stations do not necessarily provide a larger secret key rate in this case. However, note that thanks to the overall avoidance of storing qubits, there are no extra memory errors in our scheme such as the usual memory dephasing in memory-based quantum repeaters. Also note that our model to include the local imperfections exclusively via local losses means that also the finally shared state in Equations (37) and (38) maintains its specific form where only one type of Pauli errors occurs resulting in a nonzero QBER only in one of the two BB84 variables (see Equation (42)). In a more general model that takes into account other local operational errors such as qubit depolarizing errors, both QBERs become nonzero and in this case the secret key fraction may sharply drop to zero for insufficient depolarization error parameters even when all the other parameters take on very good values (see Equation (41)). However, in principle, also in this more general setting, general quantum error correction codes can provide a certain level of pro-

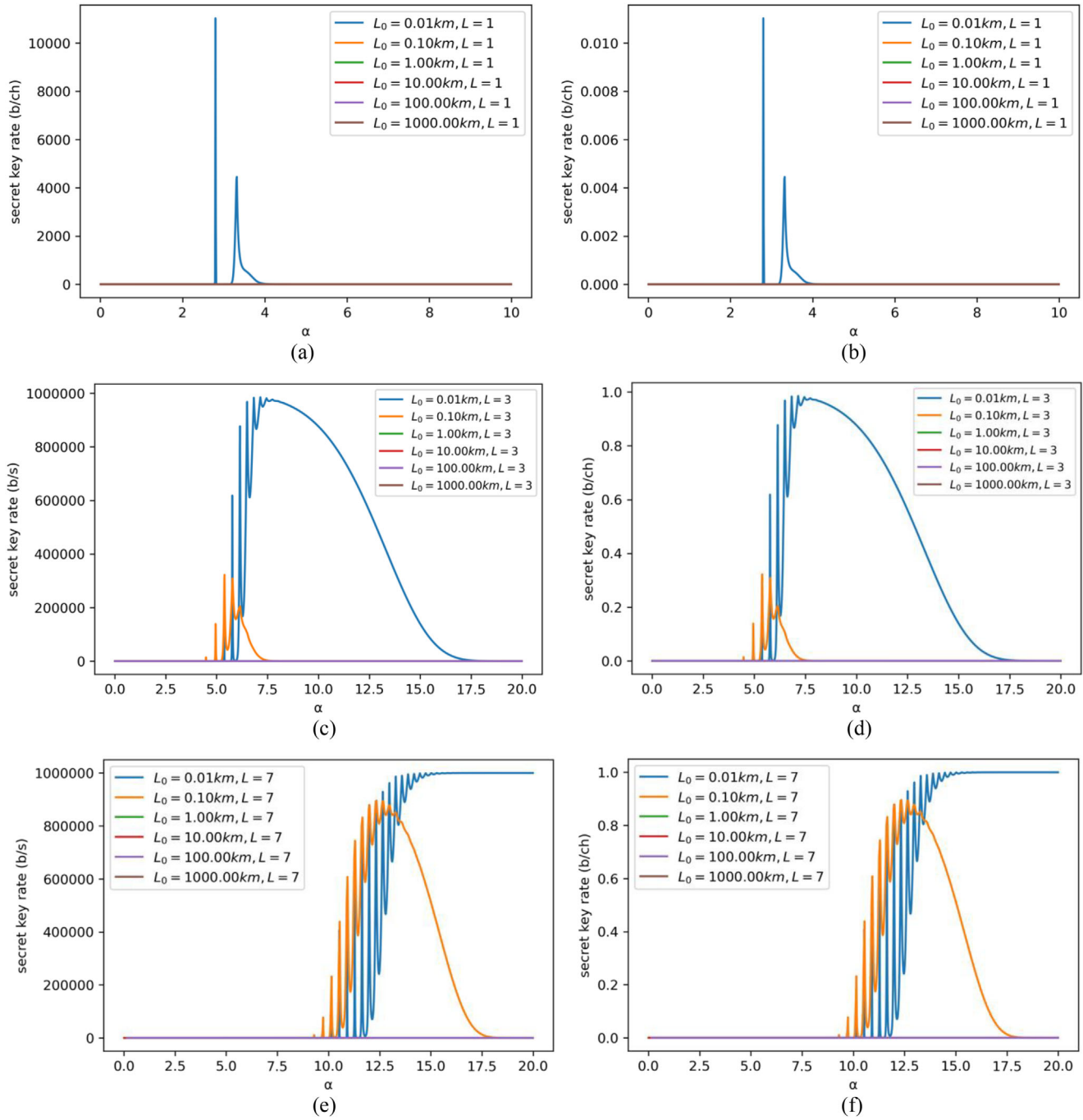


**Figure 5.** a,c,e) The lower bound of the secret key rate per second  $R_{\text{QKD}} t_0$  and, b,d,f) also explicitly shown for convenience, the secret key rate per channel use  $R_{\text{QKD}} t_0$  as a function of  $\alpha$  for codes with different loss order: 1-loss code in (a) and (b), 3-loss code in (c) and (d), 7-loss code in (e) and (f), and also for various elementary distances  $L_0$ :  $L_0 = 0.01$  km (blue),  $L_0 = 0.1$  km (orange),  $L_0 = 1$  km (green),  $L_0 = 10$  km (red),  $L_0 = 100$  km (purple), and  $L_0 = 1000$  km (brown). The total distance is always chosen to be 1000 km.

tection against such local errors. Experimentally, both local loss and local (dephasing or depolarizing) noise may occur with typically one dominating over the other.

In order to evaluate the effects caused by the local losses, we set  $\eta_{\text{local}} = 0.99, 0.999$ . In **Figure 6c,e**, one can see that the secret key rates are indeed reduced, but they would still overcome the

PLOB bound, even when the local errors are included with a loss order of  $L = 3, 7$ . For  $\eta_{\text{local}} = 0.999$ , the rates do not change a lot and we can still realize near-unit rates per channel use for certain values of  $\alpha$  and  $L_0$ . On the other hand, for  $\eta_{\text{local}} = 0.99$ , the final rates decrease greatly. However, we can see in **Figure 6d,f**, even though the rates are much smaller than unity, they can still beat

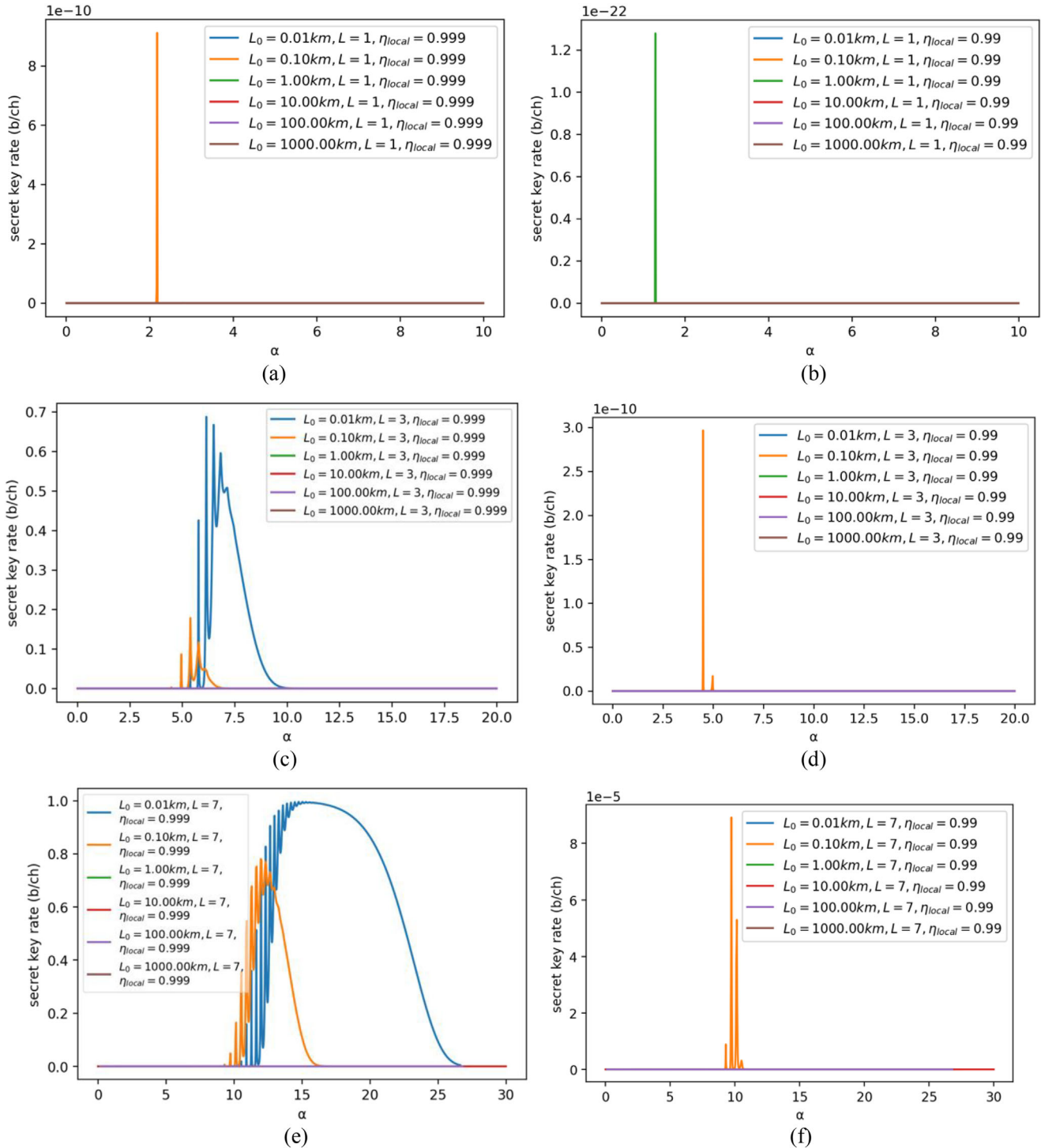


**Figure 6.** The lower bound of the secret key rate per channel use  $R_{\text{QKD}}^{\dagger_0}$  including a,c,e) local loss:  $\eta_{\text{local}} = 0.999$  and b,d,f)  $\eta_{\text{local}} = 0.99$  as a function of  $\alpha$  for codes with different loss orders: 1-loss code in (a) and (b), 3-loss code in (c) and (d), 7-loss code in (e) and (f), and also for various elementary distances  $L_0$ :  $L_0 = 0.01$  km (blue),  $L_0 = 0.1$  km (orange),  $L_0 = 1$  km (green),  $L_0 = 10$  km (red),  $L_0 = 100$  km (purple), and  $L_0 = 1000$  km (brown). The total distance is always chosen to be 1000 km.

the PLOB bound. Also, the peaks are very narrow for  $\eta_{\text{local}} = 0.99$ , so to reach the optimal secret key rates, one needs to have a pretty accurate control of the value of  $\alpha$ . As for the 1-loss code, we can see in Figure 6a,b that the rates already decrease significantly even for  $\eta_{\text{local}} = 0.999$  and there is only a narrow peak to overcome the PLOB bound. For  $\eta_{\text{local}} = 0.99$ , the rates cannot beat the PLOB bound even with very short  $L_0$ . Moreover, one can see that a shorter elementary distance  $L_0$  does not necessarily bring us a better performance of the secret key rate according to Figure 6a,b. In Figure 6a, it can be seen that the best choice for  $L_0$  is not the shortest one,  $L_0 = 0.01$  km, but instead a larger one,  $L_0 = 0.1$  km, and in Figure 6b, the best choice is even larger than that— $L_0 = 1$  km.

The secret key rate inevitably drops if the local losses are included in addition to the channel losses and a consequence is that the local losses must not be too large ( $\eta_{\text{local}} \geq 0.999$ ) in order to obtain an  $\alpha$ -regime where the secret key rate per channel use is close to unity. However, as already mentioned in Section 3.3, even though the numerical analysis for higher-loss codes beyond  $L = 7$  has not been done yet, we expect that if the loss order  $L$  could be larger ( $L > 7$ ), there should be an  $\alpha$ -regime with reasonable values of  $L_0$  (note again that the shortest  $L_0$  may not be the best choice) and also the maximally allowed local losses could be a bit larger (e.g.,  $\eta_{\text{local}} \leq 0.99$ ). Nonetheless, keeping the local imperfections at very low values ( $10^{-3}$ – $10^{-2}$  or possibly  $10^{-1}$  corresponding to a regime less demanding than for the typical threshold values in fault-tolerant quantum computing) is a requirement of our scheme which is not easy to meet in a practical realization.

### 3.5. Conclusion

We proposed a scheme for long-distance entanglement distribution based on so-called RSBCs and cavity-QED. The cavity-QED system employs a three-level atom confined in a high-finesse cavity. An exploitation of the atomic system for quantum storage is unnecessary, because our protocol, though based on spin–spin entanglement distribution, does not involve any extra classical signaling times for synchronization of the repeater segments. This is achieved by utilizing quantum error correction of photon loss errors. We showed that the cavity-QED-based approach can be used to generate the RSBC for the photonic communication through the fiber channels of the repeater. At the same time, the cavity-QED interactions can be employed to do the syndrome measurement required for loss error correction and to create the entangled atomic states. Thanks to the properties of the RSBCs, the dominating errors induced from photon losses along the optical fiber channel can be immediately corrected at the intermediate repeater stations.

A specific instance of an RSBC—the cat code has been analyzed in detail. To get a better state fidelity, generally higher-loss codes are needed. However, in this case, the overlap of the codewords increases, which results in a worse success probability of the optical, USD, as employed in our scheme to disentangle the light modes from the entangled spin states. Fortunately, we found that for higher-loss codes, fewer elementary repeater stations are required in order to get an  $\alpha$  regime ( $\alpha$  is the light mode amplitude) where both the final state fidelity and the overall success probability become near-unity. For QKD applications,

the secret key rate analysis leads to a similar conclusion, namely that for higher-loss codes, fewer elementary repeater stations are needed to obtain an  $\alpha$  regime where the secret key rate per channel use is close to unity. Final secret key rates of the order of MHz are then possible, i.e., in principle, final long-distance quantum communication rates that match the experimentally given clock rates for cavity-QED atom–light systems. However, once the local losses at all the repeater stations are included into the analysis, as required to assess a more realistic scenario, the key rate can drop dramatically for a local transmission parameter chosen too small (i.e., smaller than 0.99). Hence, really small local losses (with a local transmission greater than 0.999) must be assumed at every elementary station in our scheme to keep the key rate close to unity. Nonetheless, it is also predicted that even higher-loss codes than those considered here (i.e.,  $L > 7$ ) may lead to a further improvement.

Cat qubits could also be embedded into a higher multiqubit code,<sup>[12,17,18]</sup> e.g., the so-called quantum parity code, combining many physical qubits into a logical qubit. Unlike the usual single-photon dual-rail (two-mode) qubits for which some physical qubits are considered to be erased through the loss channel (i.e., two independently acting, identical oscillator amplitude damping channels), the single-mode qubits in bosonic, continuous-variable codes will not be naturally erased in a fiber channel. Instead, in this case, the single-mode amplitude damping generally leads to a distortion of the quantum states. Nonetheless, we may choose to discard some qubits artificially, e.g., we can do the USD on one of the physical qubits and if it turns out to be unsuccessful, we then discard this qubit and attempt the USD for the remaining physical qubits. So, with this method, in principle, we can have a higher chance to accomplish the USD and the overall success probability of such a repeater scheme will be improved. A crucial benefit of our current approach though is that it is hardware-efficient and thus no additional multimode couplings to generate the higher-order multiqubit codes are needed.

There are still various other kinds of RSBCs, e.g., those based on squeezed cat states, binomial states, or Pegg–Barnett states.<sup>[9]</sup> Our scheme for the syndrome measurement is expected to work also for the generalized RSBCs. However, the performance in terms of fidelity is no longer so clear for the other RSBCs, but the overlap of the codewords potentially becomes smaller (so the success probability is expected to be improved) than for the cat codes, especially when the squeezed cat codes and the binomial codes are considered. Thus, as a combination of the final state fidelity and the overall success probability, the secret key rate of long-range QKD based on our repeater scheme should also be improved with this generalization. To conclude, the other RSBCs potentially have a better performance than the cat codes and we leave it for future work to analyze the performance of other instances of RSBCs. Generally, we hope that our scheme will inspire further experimental research towards realizing elements of the proposed method with the ultimate goal of long-distance quantum communication. For a practical, real-world application, however, the local losses and errors that occur at every repeater station in our scheme are a serious obstacle and so further loss/error-suppressing elements would have to be incorporated into our scheme, for instance, via additional quantum error correction codes on the atomic spin qubit. Moreover, in our high-rate repeater scheme, all elements

must be precisely synchronized, especially with uneven segment lengths where additional delay lines may be employed.

## Supporting Information

Supporting Information is available from the Wiley Online Library or from the author.

## Acknowledgements

The authors thank the BMBF in Germany for support via Q.Link.X/QR.X and the BMBF/EU for support via QuantERA/ShoQC and the Deutsche Forschungsgemeinschaft (DFG, German Research Foundation) – Project-ID 429529648 – TRR 306 QuCoLiMa (“Quantum Cooperativity of Light and Matter”).

Open access funding enabled and organized by Projekt DEAL.

## Conflict of interest

The authors declare no conflict of interest.

## Data Availability Statement

The data that support the findings of this study are available from the corresponding author upon reasonable request.

## Keywords

cat states, cavity-QED, continuous variable codes, quantum communication, quantum key distribution

Received: October 26, 2022  
Revised: May 8, 2023  
Published online: June 8, 2023

- [1] H.-J. Briegel, W. Dür, J. I. Cirac, P. Zoller, *Phys. Rev. Lett.* **1998**, *81*, 5932.
- [2] P. van Loock, W. Alt, C. Becher, O. Benson, H. Boche, C. Deppe, J. Eschner, S. Höfling, D. Meschede, P. Michler, F. Schmidt, H. Weinfurter, *Adv. Quantum Technol.* **2020**, *3*, 1900141.
- [3] L. Jiang, J. M. Taylor, K. Nemoto, W. J. Munro, R. V. Meter, D. Lukin, *Phys. Rev. A* **2009**, *79*, 032325.
- [4] S. Muralidharan, L. Li, J. Kim, N. Lütkenhaus, M. D. Lukin, L. Jiang, *Sci. Rep.* **2016**, *6*, 20463.
- [5] M. Mirrahimi, Z. Leghtas, V. V. Albert, S. Touzard, R. J. Schoelkopf, L. Jiang, M. H. Devoret, *New J. Phys.* **2014**, *16*, 045014.
- [6] B. Hacker, S. Welte, S. Daiss, A. Shaukat, S. Ritter, L. Li, G. Rempe, *Nat. Photonics* **2019**, *13*, 110.
- [7] M. Bergmann, P. van Loock, *Phys. Rev. A* **2016**, *94*, 042332.
- [8] L. Li, C.-L. Zou, V. V. Albert, S. Muralidharan, S. M. Girvin, L. Jiang, *Phys. Rev. Lett.* **2017**, *119*, 030502.
- [9] A. L. Grimsmo, J. Combes, B. Q. Baragiola, *Phys. Rev. X* **2020**, *10*, 011058.
- [10] J. Hastrup, J. S. Neergaard-Nielsen, U. L. Andersen, *Opt. Lett.* **2020**, *45*, 640.
- [11] J. Hastrup, U. L. Andersen, *Phys. Rev. Res.* **2022**, *4*, 043065.
- [12] D. Su, I. Dhand, T. C. Ralph, *Phys. Rev. A* **2022**, *106*, 042614.
- [13] D. Gottesman, A. Kitaev, J. Preskill, *Phys. Rev. A* **2001**, *64*, 012310.
- [14] K. Fukui, R. N. Alexander, P. van Loock, *Phys. Rev. Res.* **2021**, *3*, 033118.
- [15] F. Rozpedek, K. Noh, Q. Xu, S. Guha, L. Jiang, *npj Quantum Inf.* **2021**, *7*, 102.
- [16] J. Hastrup, U. L. Andersen, *Phys. Rev. Lett.* **2022**, *128*, 170503.
- [17] S.-H. Lee, S.-W. Lee, H. Jeong, *Phys. Rev. Res.* **2021**, *3*, 043205.
- [18] A. P. Lund, T. C. Ralph, H. L. Haselgrove, *Phys. Rev. Lett.* **2008**, *100*, 030503.
- [19] L.-M. Duan, H. J. Kimble, *Phys. Rev. Lett.* **2004**, *92*, 127902.
- [20] B. Wang, L.-M. Duan, *Phys. Rev. A* **2005**, *72*, 022320.
- [21] Here we use the property of  $R\phi$ . It is easy to prove that  $R\phi R\psi = R\phi + \psi$ . Thus, we have  $R\pi/2R\pi = R3\pi/2$ .
- [22] Formally, the initially prepared entangled states in our scheme are for a single optical mode coupled to a single spin. Sending the optical half, the light mode, from one to another repeater station physically means that a wave packet or an optical pulse containing a certain (average) number of photons will be transmitted through the fiber channel. To keep an unambiguous and clear connection to the formal description, we mainly stick to expressions like ‘sending/receiving a mode’, which physically refers to an optical pulse that contains many photons and travels between the repeater stations.
- [23] D. Dieks, *Phys. Lett. A* **1988**, *126*, 303.
- [24] A. Peres, *Phys. Lett. A* **1988**, *128*, 19.
- [25] Here we use the relation:  $Rk\pi/2m-1\ 02m, \Theta = 02m, \Theta$  and  $Rk\pi/2m-1\ 12m, \Theta = 12m, \Theta$  for any  $K \in N_0$ . One can easily prove it from Equation (15).
- [26] I. L. Chuang, D. W. Leung, Y. Yamamoto, *Phys. Rev. A* **1997**, *56*, 1114.
- [27] B. T. Kirby, S. Santra, V. S. Malinovsky, M. Brodsky, *Phys. Rev. A* **2016**, *94*, 012336.
- [28] S. Abruzzo, S. Bratzik, N. K. Bernardes, H. Kampermann, P. van Loock, D. Bruß, *Phys. Rev. A* **2013**, *87*, 052315.
- [29] Z. Leghtas, G. Kirchmair, B. Vlastakis, R. J. Schoelkopf, M. H. Devoret, M. Mirrahimi, *Phys. Rev. Lett.* **2013**, *111*, 120501.
- [30] V. Scarani, H. Bechmann-Pasquinucci, N. J. Cerf, M. Dušek, N. Lütkenhaus, M. Peev, *Rev. Mod. Phys.* **2009**, *81*, 1301.
- [31] S. Pirandola, R. Laurenza, C. Ottaviani, L. Banchi, *Nat. Commun.* **2017**, *8*, 15043.
- [32] F. Schmidt, P. van Loock, *Phys. Rev. A* **2020**, *102*, 042614.